Electronic Supplementary Material (ESI) for Soft Matter
This journal is © The Royal Society of Chemistry 2013

Supplementary Information

1 Synthesis and characterization of the photosensitizer

The compound that we named Chlorin-12 is the second of the isomers characterized by ^{1}H-NMR (see Fig.S1), COSY, ESI-MS and UV-Vis.

2^1,2^2[*N*,*N*-dicarbonyl-*N*-(4-dodecylphenyl)]-8,12-bis[2-(methoxycarbonyl) ethyl]-2,7,13,17-tetramethyl-18-vinyl-$2,2^1,2^2,2^3$-tetrahydrobenzo[*b*]porphyrin. ^{1}H NMR ($CDCl_3$, 500 MHz), δ (ppm): -2.45 (br s, 2H, H-21 and H-23); 0.9-1.27 (m, *p*-alkyl group); 2.08 (s, 3H, CH_3-2^5), 3.17 (t, 2H, J = 8.0 Hz, H-12^2), 3.21 (t, 2H, J = 8.0 Hz, H-8^2); 3.42 (s, 3H, CH_3-13^1); 3.47 (s, 3H, CH_3-7^1); 3.45-3.48 (m, 2H, H-$2^{3\alpha}$ and H-$2^{3\beta}$); 3.61 (s, 3H, CH_3-17^1), 3.91-3.95 (m, 1H, H-2^2) 3.65 and (s, 3H, 12^4); 3.66(s, 3H, 8^4);4.18 (t, 2H, J = 8.0 Hz, H-12^1); 4.32 (t, 2H, J = 8.0 Hz, H-8^1); 4.65 (d, 1H, J = 8.5 Hz, H-2^1); 6.10 (dd, 1H, J = 11.5 and 1.5 Hz, H-$18^{2\alpha}$); 6.33 (dd, 1H, J = 18.0 and 1.5 Hz, H-$18^{2\beta}$); 6.99-7.01 (m, 2H, H-2^9 and 2^{13}); 7.41 (t, J = 5.0 Hz, 1H, H-2^4); 7.73-7.70 (m, 2H, H-2^{10} and H-2^{12}); 8.13 (dd, 1H, J = 18.0 and 11.5 Hz, H-18^1); 9.26 (s, 1H, H-5); 9.28 (s, 1H, H-20); 9.68 (s, 1H, H-10), 9.74 (s, 1H, H-15).

ESI-MS-TOF, m/z 933.5321 calculated for $C_{58}H_{70}N_5O_6^+(MH^+)$; found 933.5329.

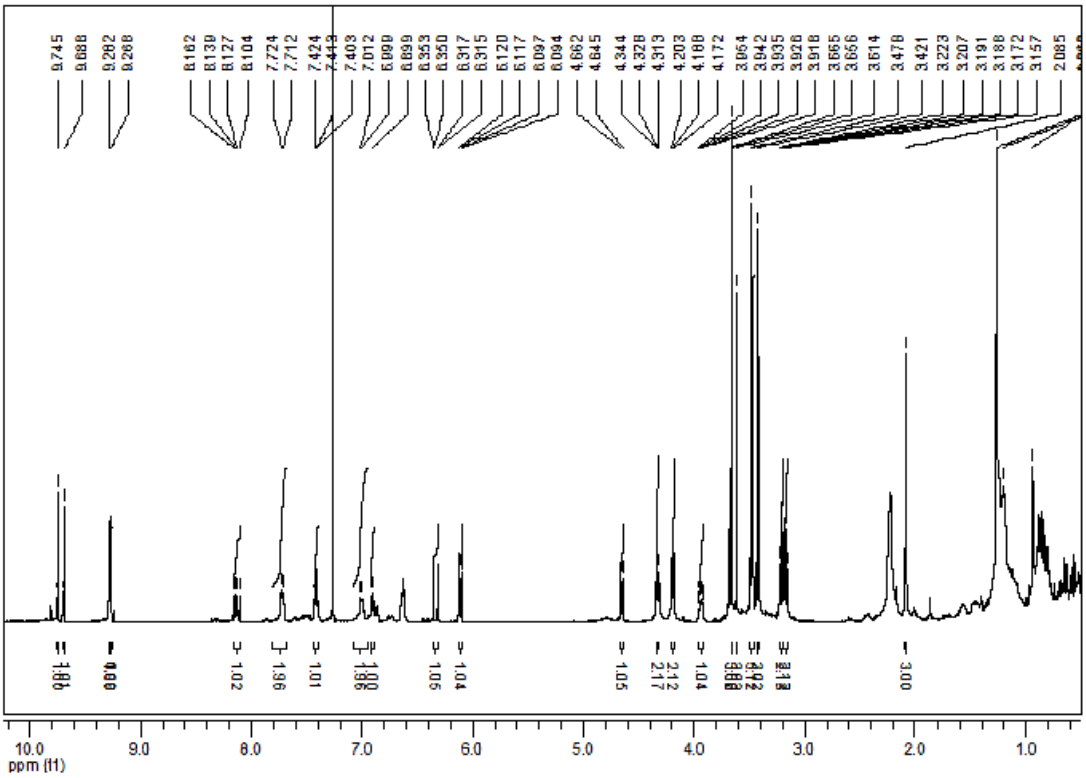

Figure S1: ^{1}H-NMR (500 MHz) in $CDCl_3$ of Chlorin-12.

2 Langmuir monolayer

We performed Langmuir isotherms on pure POPC and pure POPC-OOH molecules (see Fig. S2). Precautions were taken in order to avoid oxidation of the monolayers exposed to laboratory air by working under controlled N_2 atmosphere. POPC-OOH shows clearly values of area per molecule (APM) which are larger than POPC.

Defining $\Delta A/A$ as

$$\frac{\Delta A}{A} = \frac{APM_{POPC-OOH} - APM_{POPC}}{APM_{POPC}}, \tag{1}$$

we measure $\Delta A/A \sim 50\% at low pressure$, in agreement with the observations of van den Berg et al. [1] who compared PLPC monolayers with PLPC-OOH monolayers. Fig. S3 represents the

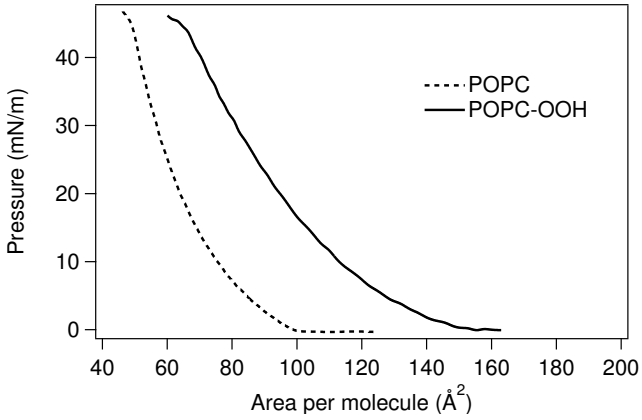

Figure S2: Langmuir isotherms at 20°C of monolayers made of mixtures of POPC (dashed line) and of the hydroperoxidized form POPC-OOH (full line).

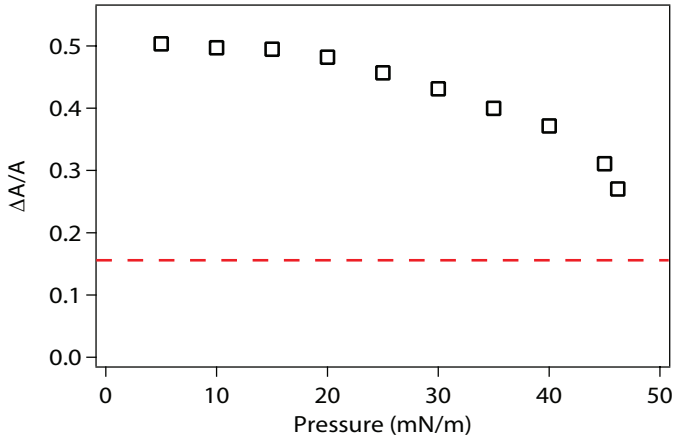

Figure S3: $\Delta A/A$ as a function of the pressure Π (□). The dashed line corresponds to the relative area difference between POPC and POPC-OOH in bilayers.

evolution of $\Delta A/A$ as a function of the surface pressure Π. This relative area difference decreases as the pressure increases. For the maximum pressure that we can achieve, $\Delta A/A$ decreases to 27%. Thus, whatever the pressure, $\Delta A/A$ remains larger than the relative area increase measured in fully oxidized POPC bilayers ($\sim 15\%$).

Despite intrinsic structural differences between monolayers and bilayers, it has been shown that for a certain lateral pressure, around 30-35 mN/m, the hydration state of both monolayer and bilayer systems is identical and structural parameters of these systems are comparable [2,3]. The use of monolayers to predict bilayer properties seems reasonable provided that bilayers can be pictured as two back-to-back monolayers interacting non-specifically as two slabs [4]. Depending on the properties one focuses on, the monolayer / bilayer equivalence occurs at different pressures. In the case of relative area increase between POPC and its hydroperoxidized form POPC-OOH, even if there is no pressure value that allows to reach the monolayer / bilayer equivalence, our results clearly show a larger area per molecule of the hydroperoxidized form of the lipids in qualitative agreement with area increase in the bilayers.

3 Experiments analysis

3.1 Control experiments

3.1.1 Start-Stop experiments

We performed start-stop experiments on the decorated GUVs, hold by the micropipette, by irradiating the sample for 10 seconds, and then observing the vesicles under the DIC observation mode for 15 seconds. No delayed effects could be detected, either after stopping or after restarting irradiation. Under our conditions, there is thus an instantaneous response of the vesicle area expansion to the irradiation.

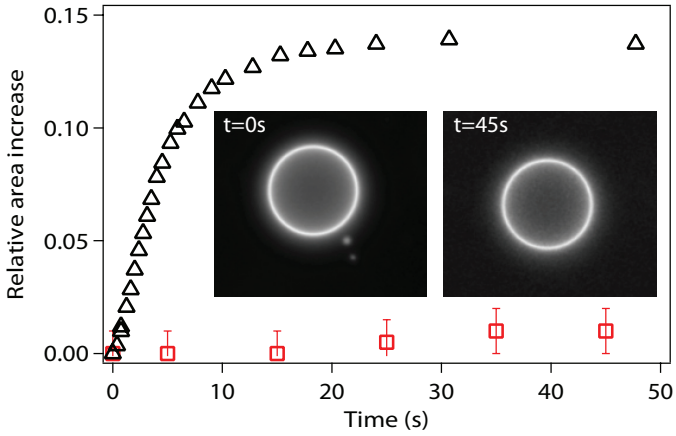

Figure S4: Evolution of the area increase in a DMPC vesicle with 1% of Chlorin-12 (□) under light irradiation and the corresponding fluorescence images, compared to the POPC vesicle showed before (△). Saturated lipids are not oxidised by singlet oxygen.

3.1.2 Singlet oxygen does not oxidise saturated lipids

We have checked that oxidation phenomena is not present for lipid chains without unsaturated bonds. We prepared GUVs made of DMPC (a lipid with two saturated chains of 14 carbons) incorporating also 1% of Chlorin-12. The liquid/gel transition temperature of DMPC is 23°C. Thus, vesicle formation has been performed in an oven at 28°C. Irradiation of the DMPC giant vesicles showed no membrane transformations. Fluorescence from Chlorin-12 molecules followed the same time evolution due to bleaching, but no enhanced fluctuations or tube/bud formation was observed. A simple image analysis, using a 2π average radial profile was enough to extract the vesicle area evolution. Fig. S4 clearly shows no area increase.

3.2 Correction of the apparent area increase

During our irradiation experiments one measures an overall increase of the apparent surface area of a GUV submitted to a constant membrane tension, applied through the micropipette device. At constant tension, a measure of area increase due to lipid peroxidation is also perturbed by the changes of the stretching modulus of the membrane. Here, we correct for such (minor) perturbations by considering first the Evans-Helfrich equation for α, the apparent area increase of a membrane submitted to a given tension σ, as a function of its constitutive mechanical parameters, the bending modulus k_c and the elastic modulus K_A

$$\alpha = \frac{k_B T}{8\pi k_c} \ln(\frac{\sigma}{\sigma_0}) + \frac{\sigma}{K_A}, \tag{2}$$

where σ_0 is a constant. In the present case, the membrane is submitted to a constant tension σ, and after a time t of illumination, a fraction x_{ox} of the lipids have been peroxidized, leading to a relative area increase $x_{ox}\epsilon$, where ϵ is the relative molecular area increase, and to a decrease of both k_c and K_A. We have measured a linear decrease of K_A with x_{ox} and noticed, without being able for technical reasons to measure it precisely, a decrease in k_c. Then, Eq. (2) becomes, after an irradiation time t

$$\alpha(x_{ox}) = \frac{k_B T}{8\pi k_c^{\text{eff}}(x_{ox})} \ln(\frac{\sigma}{\sigma_0}) + \frac{\sigma}{K_A^{\text{eff}}(x_{ox})} + x_{ox}\epsilon \tag{3}$$

with $K_A^{\text{eff}}(x_{ox}) = K_A(1 - x_{ox}) + K_A^{ox} x_{ox}$, where K_A^{ox} is the bending modulus of a completely peroxidized membrane that we have measured. The maximum error is expected for a fully peroxidized membrane. Assuming a decrease of a factor of four for k_c, $k_c^{ox} = 0.25\ k_c$, similar to that measured for K_A, $K_A^{ox} = 0.25\ K_A$, it follows that the error on the relative area increase $\epsilon(x_{ox} = 1)$, is less than 1% for a membrane submitted to a tension σ =0.7 mN m^{-1}. Notice that the relative error remains smaller than one percent if k_c^{ox} assumes values in the range $0.25\ k_c < k_c^{ox} < k_c$.

3.3 Data Analysis

GUVs decorated with various surfaces concentrations of Chlorin-12 under continuous irradiation at 410 nm, show a typical fluorescence intensity decrease due to photobleaching. We computed

This journal is © The Royal Society of Chemistry 2013

the cumulative intensity as the integral over time of the fluorescence signal. For a given quantum yield for $^1O_2$ production ϕ_Δ, the cumulative fluorescence is thus directly proportional to the number of $^1O_2$ species produced since the beginning of the irradiation. In the absence of bleaching, the cumulative intensity should grow linearly with time. The decrease of light intensity associated with photobleaching results in a sublinear variation of the cumulative light intensity with time. The constant of proportionality between emitted light intensity and singlet oxygen generation can be computed by noticing that the rate of singlet oxygen production Q is given by [5] $Q = \phi_\Delta \lambda P_w \sigma / hc$, where λ is the wavelength of the irradiation light (410 nm), P_w the power density, σ the cross section of absorbance, h the Planck's constant, and c the speed of light. For Chlorin-12, $\phi_\Delta = 0.63$ and $\sigma(410\text{ nm}) = 2.1$ Å^2. Thus, in our setup, each non-bleached Chlorin-12 has a production rate Q=740 molecules of $^1O_2$ per second. The associated relative area increase was measured on each vesicle by a direct analysis of the vesicle dimensions on the fluorescence images, for different irradiation times and further corrected for K_A decrease as explained above.

4 $^1O_2$ Sources, diffusion and reactions

4.1 Computing $^1O_2$ distribution

The concentration of $^1O_2$ near the plane of anchored sensitizers can be computed by solving the reaction-diffusion equation for the distribution of $^1O_2$ species:

$$\frac{\partial C_{SO}}{\partial t} = D\frac{\partial^2 C_{SO}}{\partial z^2} - \frac{C_{SO}}{\tau} + Q\Sigma\delta(z-b) \tag{4}$$

where C_{SO} is the singlet oxygen concentration profile, D the diffusion coefficient, z the distance away from the membrane, τ the $^1O_2$ lifetime, Q the rate of $^1O_2$ generation per sensitizer molecule and Σ the number of sensitizers per unit area. b is the distance from the $^1O_2$ generation plane from the membrane, of order of a fraction of nanometer. Eq. 4 supposes that singlet oxygen reactions with the unsaturated bonds only marginally perturb the distribution, a full description would require a sink term located at the average (negative) height of the double bond plane. The stationary solution of Eq. 4 reads

$$C_{SO}(z) = \frac{Q\tau\Sigma}{2\ell_D}\exp\{-\frac{z}{\ell_D}\}. \tag{5}$$

Close to the generating wall there is thus a concentration of singlet oxygen given by

$$C_{SO}(z=0) = 0.5Q\tau\Sigma\ell_D^{-1}. \tag{6}$$

Under our irradiation conditions and for a Chlorin-12 molar fraction of 0.03 %, where $Q = 740\text{ s}^{-1}$, $\ell_D = 100$ nm, $\tau = 4$ μs, we have $C_{SO}(z=0) = 12$ nM. It is also worth stressing that the planar localization of the sensitizers might lead to oxygen depletion if the sensitizer surface density Σ is too large. A higher bound value for $\Sigma_{\max}$ can be estimated based on the comparison between the concentration of singlet oxygen at the surface $C_{SO}(z=0)$ and the concentration of molecular oxygen in solution C_{O2}, giving $\Sigma_{\max} = 2C_{O2}\ell_D Q^{-1}\tau^{-1}$ and a maximum sensitizer fraction $f_{\max} = \Sigma_{\max} S_0$ where S_0 is the area of one lipid molecule. Under our conditions where S_0 =0.65 nm^2, and C_{O2} =250 μM, we get $f_{\max}$ of order unity. In our case, where $f_{\max} \ll 1$, $^1O_2$ generation should thus not be limited by oxygen depletion effects.

4.2 Inhomogeneities in singlet oxygen distribution

The smallest average time interval between two successive $^1O_2$ generation events being, under our irradiation conditions, of order of 1.4 ms, the sensitizer diffuses in this interval over a typical distance of 20 nm. The distance between two probes is explored in 7 ms by the photosensitizer diffusive motion, corresponding to 5 emission events; during the time of the experiment, which is of order of one minute, each photosensitizer diffuses thus over distances one hundred times larger than the inter-probe length further contributing to an homogeneous distribution of $^1O_2$ species. These homogenizing factors are even stronger for the surface densities of the samples with high probe fractions such as the 2 % mol case shown in the main text, where the average distance between sensitizers is smaller than 10 nm. However, in this denser case, the average distance between sensitizers is comparable with the length below which self-quenching becomes significant [6], we thus confined our quantitative efficiency measurements to samples with lower probe densities, as discussed in the next paragraph.

4.3 Equivalent bulk constants for the hydroperoxidation reaction

Photosensitizers generate an average concentration of $^1O_2$ species close to the membranes given by $C_{SO} = 0.5\Sigma Q\tau\ell_D^{-1}$, where Q is the number of $^1O_2$ generated per photosensitizer by unit time, Σ the number of photosensitizers per unit surface and τ the $^1O_2$ lifetime. The factor 0.5 relies on the assumption that $^1O_2$ molecules distribute evenly on both sides of the probe plane. In a binary reaction between $^1O_2$ species at a concentration C_{SO} and double bonds of concentration C_{DB} one creates $k_{HP}C_{DB}C_{SO}$ hydroperoxide species per unit time $dC_{HP}/dt = k_{HP}C_{SO}C_{DB}$. Associating m, the initial slope of the curve in Fig. 4 (main text), with the value for the relative rate production of -OOH groups, $m = C_{DB}^{-1}dC_{HP}/dt|_{t=0}$ one has $k_{HP} = m \times C_{SO}^{-1}$. For the case of Fig. 4 in the main text, $m = 0.036$. With $Q = 740$ s^{-1}, $\ell_D = 100$ nm, $\tau = 4$ μs and $\Sigma = 4.7 \times 10^{-4}$ nm^{-2}, this leads to the reaction constant value $k_{HP} \simeq 3 \times 10^6$ M^{-1}s^{-1}.

5 Single Chain Mean Field theory

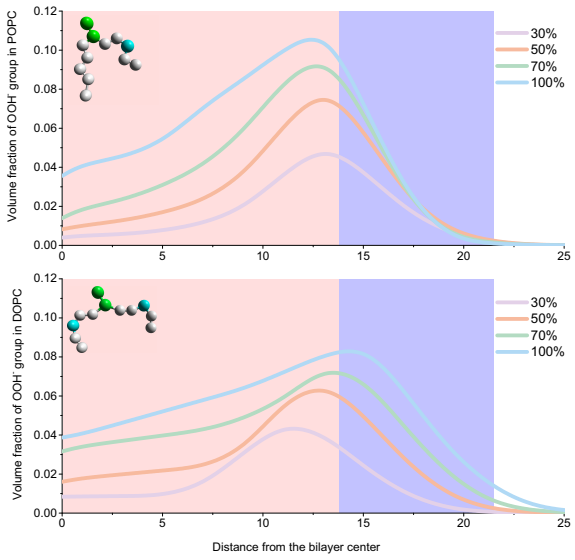

Figure S5: Averaged position of the oxidized beads in POPC bilayer (top) and DOPC bilayer (bottom) as a function of the distance from the center of the bilayer for different rates of oxidation. Rose band corresponds to the hydrophobic core of the bilayer, while blue band corresponds to the heads region. Typical configurations of the oxidized lipids are shown in the inset.

Lipid molecules are modeled within the Single Chain Mean Field theory [7]. This theory is shown to describe adequately equilibrium and mechanical properties of lipid bilayers using coarse-grained models for lipid molecules [7]. Since mechanical and equilibrium properties of DOPC and POPC lipid bilayers, such as thickness, compressibility and the area per lipid are very close to each other, we describe both DOPC and POPC lipid bilayers using unique 10-beads model shown in Fig. 5 of main text. The oxidized DOPC and POPC molecules are described with the same set of parameters as non-oxidized lipids, but the central hydrophobic bead of the tail (grey), which corresponds to the double bond, is replaced by a hydrophilic bead (cyan), which has interactions with solvent two times less than the beads of the heads (green) (see Fig. S5). Our SCMF calculations have shown that more hydrophilic OOH group migrates closer to the surface, forming a kink in the tails. The oxidized beads stay at the border between hydrophobic core and the heads region. These groups, in turn, distort the bilayer, preventing close packing of neighboring tails, which is probably the main effect of oxidation. Although the peak of average position of OOH groups is slightly displaced to the surface of the bilayer (Fig. S6), some OOH groups can be found outside of the bilayer (Fig. S6).

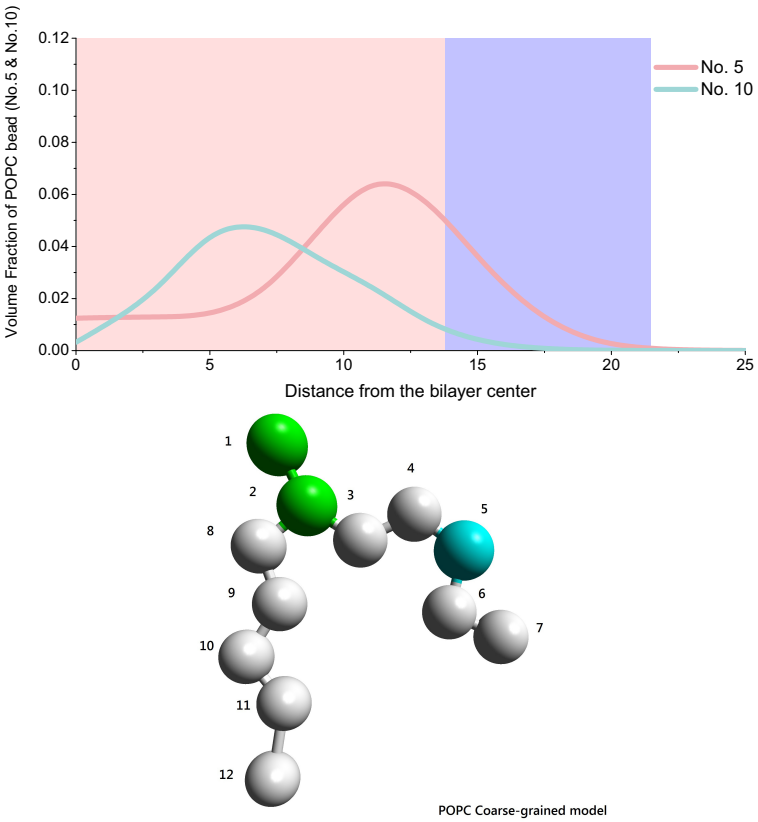

Figure S6: Averaged position of oxidized OOH group (bead N° 5) and symmetrical carbon group (bead N° 10) of POPC oxidized lipid in the bilayer.

References

[1] J J van den Berg, J A Op den Kamp, B H Lubin, and F A Kuypers. Conformational changes in oxidized phospholipids and their preferential hydrolysis by phospholipase a2: a monolayer study. *Biochemistry*, 32(18):4962–7, May 1993.

[2] J. Brewer, J. Bernardino de la Serna, K. Wagner, and L. A. Bagatolli. Multiphoton excitation fluorescence microscopy in planar membrane systems. *Biochimica and Biophysica Acta*, 1798:1301Ð1308, 2010.

[3] D Marsh. Lateral pressure in membranes. *Biochim Biophys Acta*, 1286(3):183–223, Oct 1996.

[4] J.F. Nagle and S. Tristram-Nagle. Structure of lipid bilayers. *BBA Biomembranes*, 1469:159–195, 2000.

[5] N. A. Busch, M. L. Yarmush, and M. Toner. A theoretical formalism for aggregation of peroxidized lipids and plasma membrane stability during photolysis. *Biophys J*, 75(6):2956–2970, Dec 1998.

[6] Joseph R. Lakowicz. *Principle of fluorescence spectroscopy*. Springer, 3rd edition, 2006.

[7] Sergey Pogodin and Vladimir A. Baulin. Coarse-grained models of phospholipid membranes within the single chain mean field theory. *Soft Matter*, 6(10):2216–2226, 2010.